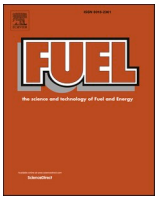
Fuel 343 (2023) 127905



Contents lists available at ScienceDirect

Fuel

journal homepage: www.elsevier.com/locate/fuel





The impact of turbulence and combustion models on flames and emissions in a low swirl burner

Mehmet Salih Cellek [a], Ali Pınarbaşı [b], Gokhan Coskun [c,*], Usame Demir [d]

[a] Department of Mechanical Engineering, Bingöl University, Bingöl, Turkey
[b] Department of Mechanical Engineering, Yıldız Technical University, İstanbul, Turkey
[c] Department of Mechanical Engineering, Sakarya University, Sakarya, Turkey
[d] Department of Mechanical Engineering, Bilecik Şeyh Edebali University, Bilecik, Turkey

ARTICLE INFO

Keywords:
Low swirl boiler
Natural gas
CFD
Turbulence model
Combustion model

ABSTRACT

Since natural gas fuel boilers are environmentally friendly and efficient, they are widely used in heating systems today. Improvements are continuing in the combustion efficiency and emissions of these boilers. Due to the high costs and long manufacturing times, experimental studies are progressing slowly. For this reason, studies with CFD simulations are also preferred. For realistic CFD results, it is important to correctly choose the turbulence and combustion models. This study conducted an experimental study to obtain temperature and emission measurements from a low-swirl natural gas boiler. Then, CFD simulations were made under the same conditions using the 3D model prepared for the same boiler. In simulation studies, different turbulence and combustion models were investigated. The turbulence models used in the simulations are Standard k-ε, Realizable k-ε, RNG k-ε, and Reynolds Stress Model (RSM), respectively. Combustion models are Eddy Dissipation (ED), Finite Rate/Eddy Dissipation (FR/ED), Eddy Dissipation Concept (EDC), Non-Premix Combustion (NPC) and Partial-Premix Combustion (PPC). When the results obtained by numerical simulations are compared with the experimental data, it is understood that the Realizable k-ε turbulence model provides better convergence than other turbulence models, while PPC and ED provide better convergence in combustion models. Since the two-step chemical mechanism for natural gas used in EDC and FR/ED models neglects the formation of many intermediate products, higher NOx values were obtained than the experimental for these combustion models. Different results were obtained from the standard k − ε in terms of temperature and CO_2, H_2O, O_2, CO, NO_x results than other turbulence models.

1. Introduction

Although renewable energy and nuclear energy are one of two fastest-growing energy sources and the consumptions are expected to increase by an average 2.6%/year and 2.3%/year between 2012 and 2040 respectively, fossil fuels will fulfill 78% of energy use in 2040. As for fossil fuel, global natural gas consumption will grow in the long term by 1.9%/year, liquid fuels consumed for transportation will increase by an average of 1.1%/year, and the coal that is the world's slowest-growing energy source will rise by an average of 0.6%/year, from 2012 to 2040 [1].

Advantage of the gaseous fuel than solid and liquid fuels is that it is easier to control combustion emissions, and has lower costs to set-up and operates with higher efficient devices [2,3]. Natural gas is the most consumed fuel in today's world [4] because of its abundance in the world, and it is commonly used in many areas [5]. Natural gas is used in a wider range than other flammable gases due to its properties such as the amount of presence in nature, the possibility of being in different geographical regions, and less harmful to nature. For these reasons, natural gas boilers are frequently preferred for heating systems in residences and industries [6,7]. In order to increase the efficiency and reduce the emissions of natural gas boilers, studies are carried out with experimental and simulation methods [8–10]. At high temperatures regions experimental measurements with thermocouples may occur some problems [11–15]. Simulation studies are preferred because experimental studies are costly and require long-term manufacturing processes. However, it is known that the results obtained from the combustion simulations with CFD differ according to the mesh number,

* Corresponding author at: Department of Mechanical Engineering, Sakarya University, Sakarya, Turkey.
E-mail address: gcoskun@sakarya.edu.tr (G. Coskun).

https://doi.org/10.1016/j.fuel.2023.127905
Received 29 December 2022; Received in revised form 1 February 2023; Accepted 18 February 2023
Available online 28 February 2023
0016-2361/© 2023 Elsevier Ltd. All rights reserved.



Fig. 1. ECO 45 G C 3B burner and boiler used for experimental study.

Table 1
Experimental devices and the uncertainty values.

Measured parameter	Measured devices	Range	Accuracy
$\dot{Q}_{gas}$	Sensyflow iG	Maks. 6500 Nm^3/h	±% 0.3
$\dot{Q}_{cooling\ water}$	ProcessMaster300	Maks. 600 m^3/h	±% 0.4
O_2	NOVA plus	% 0–21	±% 0.2
CO	NOVA plus	0–300 ppm	± 2 ppm
CO	NOVA plus	0–4000 ppm	± 100 ppm
CO_2	NOVA plus	% 0–3	±% 0.5
NO	NOVA plus	0–300 ppm	± 2 ppm
NO	NOVA plus	0–1000 ppm	± 5 ppm
NO_2	NOVA plus	0–200 ppm	± 5 ppm
CH_4	NOVA plus	% 0–3	±% 0.03
T_{air}	NOVA plus	0–100 °C	± 1 °C
T_{gas}	NOVA plus	0–650 °C	±2°C
Calculations			Uncertainty
$\dot{Q} = \dot{m}H_u$			±% 0.3
NOx			± 5.38 ppm

selected turbulence, and combustion models. In this respect, there are studies in the literature to obtain accurate results for different combustion applications [16].

In recent times, some of objectives of researchers related to area of combustion are to introduce the fuel characteristics and combustion behavior [17,18] chemical kinetic mechanism (detailed, skeletal and reduced) and its modelling [19,20] computational fluid dynamics (CFD) modelling and validation [21,22], low emission eco-friendly alternative fuels [23,24], control the combustion flame [25,26,27] and noise [28] so that improve the design of environment friendly burner [29,30], furnaces, boilers, gas turbine combustor and combustion chamber by taking into consideration less energy consumption, reduce the combustion generated pollutants, and control the combustion noise. Besides intensive experimental studies maintained by many researchers for much more specific cases, on the other hand, recent development in computer technology on high-performance computing clusters, Computer-Aided Design (CAD) and Computational Fluid Dynamics (CFD) lead to specific important facilities to design of any machines or investigate the complex and the high turbulence internal flows. CAD and CFD allow not only interpreting design procedure and the internal flow but also enable optimizing the product components with less cost and waste of time before the manufacturing stage.

Silva et al. [17,31] performed CFD simulation by accepting natural gas as methane in a 2D axisymmetric cylindrical combustion chamber. They used the Eddy Breakup – Arrhenius model with a two-step reaction mechanism. In this study, they simulated the natural gas combustion using the Eddy Breakup – Arrhenius model with a two-step methane-air chemical mechanism. In this approach, the wavelength depends on the gas properties in that region. These gas properties are analyzed with the Weighted-Sum-of-Gray-Gases-Model (WSGGM). Combustion chamber differential equations are solved by the volumetric control approach. In the study, they simulated experimental data obtained from the literature. The results of CH_4, T, O_2, CO and CO_2 in the combustion chamber were compared for two cases in the axial and radial directions. They noted that differences were observed between the two states throughout the combustion chamber, and there were significant differences, especially for CO2. However, it was stated that the numerical and experimental results were in good agreement with each other at a distance of 1.1 m from the point where the reactants were injected. Ren et al. [32] simulated a non-premixed methane-air flame with EDC and PDF combustion models. They used detailed and reduced mechanisms to compare mechanisms and combustion models. From this study, the results show that each combustion model agreed well with the full and reduced mechanisms. Furthermore, they found that EDC predicted a thinner flame with a higher flame temperature than PDF. When they compared to experimental data, EDC significantly over-predicted the temperature and OH fields. Also, this study showed that PDF model yields predicted more accurately in the upstream locations than EDC.

In addition to the effects of combustion models, there are various studies dealing with the effect of different turbulence models on the CFD solution for non-premixed flames. Frassoldati et al. [33] compared the effect of Reynolds Stress Model (RSM), standard k-ε and modified k-ε turbulent models on methane/hydrogen flame in slow combustion regime. According to the results they obtained, the RSM and modified k-ε models showed good agreement with the experimental results, while the standard k–ε model under predicts the jet penetration. Because the RSM model increases the computational time, they continue simulations using the modified k-ε turbulent model. Ziani et al. [34] numerically modeled the non-premixed turbulent combustion of CH_4-H_2 fuel mixture using the Probability Density Function (PDF) approach. CFD simulations were done with three different turbulence models k-ε, modified k-ε and RSM. As a result, they concluded that the modified k-ε turbulence model is suitable for simulating such flames. Pfeiler and Raupenstrauch [35] investigated the performance of realizable k-ε and RSM turbulence models. They applied different turbulence models on 2D axisymmetric and 3D CFD simulations of a non-premixed methane flame surrounded by co-flowing air. They obtained similar results between realizable k-ε 2D flame simulation and 3D RSM simulation. However, their results had some differences in turbulence and temperature field with experimental data. Therefore they modified turbulence model constants to get a better approximation. Khaldi et al. [36] carried out a numerical study to investigate the flow field, combustion, and temperature characteristics of a tangentially fired pulverized-coal furnace. Different turbulence models were used to validate the simulation results with experimental data. Their study determined that the RNG k-ε model is more suitable for estimating velocity and temperature fields. The literature research shows that each turbulence model can give good results in different applications. It is concluded that it is difficult to reveal the best turbulence model by generalizing. For this reason, more studies need to find the proper turbulence and combustion model for different combustion processes CFD simulation. This study aims to determine the most suitable turbulence and combustion models for low-swirl burner simulations. Simulation results obtained with different turbulence and combustion models were compared with experimental data.

2. Experimental procedure

The experimental study was carried out using a circular-shaped natural gas boiler with ECO 45 G C 3B burner, shown in Fig. 1 [37]. In the experimental study, the thermal load of the burner was determined by measuring the natural gas flow rate and the airflow rate

entering the burner. The thermal load is fixed to be 1085 kW with natural gas and airflow in a steady regime. During the experimental study, the excess air coefficient was fixed at $\lambda = 1.20$. During the combustion process, emissions and temperature values were measured. CO_2, O_2 and NOx emissions, temperature, and excess air values were measured with a NOVA measuring device.

The devices used in the experimental setup and the uncertainty values in the operating range are given in Table 1. In addition, the burner thermal load and NOx emission results calculated with the measurements are indicated in the same table.

3. Numerical model

3.1. Modeling of turbulent flow

Turbulent flows have attracted the attention of many researchers because of their complexity. In reality, it is very difficult to model these flows because turbulent flow is complex, random and changes instantaneously. However, today, turbulent flows can be modeled and predicted approximately in applications with CFD. Therefore various turbulence models have been developed for CFD calculations. One of the well known turbulence models is k-ε. Some of the turbulance models developed from k-ε are Standard k-ε model, Realizable k-ε model and RNG k-ε. In k-ε model, k represents turbulent kinetic energy and ε represents the dissipation rate. The main differences between the standard k-ε model, the Realizable k-ε model and the RNG k-ε models are the method of calculating the turbulent viscosity, the Prandtl numbers related to the k-ε turbulence propagation, and the production and consumption terms in the ε equation [38].

The standard k-ε model is the simplest and most basic model in which two equations define turbulence. In this model, turbulence velocity and length scale can be determined independently by solving two separate transport equations. This model, proposed by Launder and Spalding [39], has been using to solve many turbulent flow problems due to its accuracy and short solution time. Although it is a semi-empirical model, it is preferred for modeling jet and channel flows. Over time, the deficiencies in the k-ε model were identified, and by making corrections and additions, two separate k-ε models were developed as Realizable k-ε and RNG k-ε models.

The Standard k-ε model is not a good choice for modeling high eddy and swirl turbulent flows as like burners and burners of turbomachinery. Using the Realizable k-ε model is more appropriate, which can better converge to such turbulent flows. This model is recommended to be used for low swirling flow ($S < 0.5$) [40].

Like the Realizable k-ε, the other model derived from the Standard k-ε is the RNG k-ε model [41]. It is recommended to use this model instead of Standard k-ε in swirl and cyclone burners. In this model, the analytical derivative gives results using different constants than in the Standard k-ε model. It also includes different and additional terms for k and ε in the transport equation [42].

Unlike the realizable k-ε and RNG k-ε turbulence models, the RSM is recommended for high swirl number flows ($S > 0.5$) [43]. It is stated that the RSM is more successful than the other two methods in detecting the reverse flow gradients. In addition, it is stated that because of the stress terms in RSM equations, velocity profiles can predict more realistically in low-velocity counterflow regions where the flow behaves anisotropically. The handicaps of this model are difficulties in convergence and longer solution time than other models [40].

3.2. Combustion modelling

The solution of the conservation equations for chemical species is estimated by solving the local mass fraction of each species, the convection–diffusion equation for each species with the Fluent. The general form of the conservation equation is expressed as [43];

$$\frac{\partial}{\partial t}(\rho Y_i) + \nabla \bullet (\rho \vec{v} Y_i) = -\nabla \bullet \vec{J}_i + R_i + S_i \quad (1)$$

The first term on the left side of the equation represents the rate of the change, and the second term is the species' net rate of flow (convection). The first term on the right side represents the rate of change due to diffusion, here R_i is representing the net production rate of production of species i, by chemical reaction and expresses the rate of change due to other sources [43].

In the conservation equation of chemical species, the reaction rate R_i is calculated in three ways: laminar finite-rate model, eddy dissipation model, and eddy dissipation concept [43].

Gaseous fuels tend to burn quickly and the turbulent mixture controls the overall reaction rate. In non-premixed flames, turbulence mixes the fuel and oxidizer within the reaction zone. In premixed flames, turbulence slowly mixes cold reactants and hot products in the reaction zone. In some applications, the mixing is limited, complex, and sometimes unknown, so the chemical kinetic rate can be safely neglected. In the Fluent, the turbulence-chemistry interaction model is based on the work of Magnussen and Hjertager [14], known as the eddy dissipation model. This model assumes that the chemical reaction occurs much faster than reactants mixing, which mainly depends on the turbulence. In this approach, the net rate of production of species i due to reaction r, R_i, is given by the smaller of the two expressions below [43]:

Based on mass fraction of reactants:

$$R_{i,r} = \nu'_{i,r} M_{\omega,i} A \rho \frac{\epsilon}{k} min\left(\frac{Y_R}{\nu'_{R,r} M_{\omega,R}}\right) \quad (2)$$

Based on mass fraction of products:

$$R_{i,r} = \nu'_{i,r} M_{\omega,i} A B \rho \frac{\epsilon}{k} \frac{\sum P Y_P}{\sum_j^N \nu''_{i,r} M_{\omega,j}} \quad (3)$$

K turbulence kinetic energy, ε turbulence dissipation rate, Y_P and Y_R mass fraction of species, A Magnussen constant for reactants (default 4.0), B Magnussen constant for products (default 0.5), $M_{\omega,i}$, molecular weight, (R), reactants and (P), products [38]. In Equations 5 and 6, the chemical reaction rate is controlled by the large-eddy mixing time scale k/ε, as in the Spaldings' Eddy Break-up combustion model [44]. Combustion develops with turbulence ($k/\varepsilon > 0$) and there is no need for an igniter to start the combustion. This situation is valid for non-premixed flames. But in premixed flames, the combustion reactions begin at the inlet of the calculation zone. To prevent this situation, the software provides Finite-Rate Eddy Dissipation model. Here, both Arrhenius and eddy dissipation reaction rates are calculated, and the net reaction rate is taken as the minimum of these two rates [43]. This model can be used for various systems, but model constants A and B must be empirically adjusted for each reaction. The default values of 4 and 0.5 are set for one- and two-step reactions, respectively [45].

The Eddy Dissipation Concept model is an enhanced version of the Eddy Dissipation model and includes chemical mechanisms in turbulent flows. This model assumes that the reaction takes place in a fine-scale turbulence. The Eddy Dissipation Concept model includes chemical mechanisms in turbulent reaction flows [38]. However, the solution of multi-reaction chemical mechanisms is always difficult and needs longer solution times. For this reason, it usually needs to use reduced mechanisms in CFD simulations to shorten the solution time.

The non-premixed combustion model covers the solutions of the transport equations for the mixture fractions. This model does not solve one equation for each species. Instead, the mixed fractions for which the concentrations of the species are estimated are pre-calculated. The interaction of combustion chemistry and turbulence is considered with the Probability Density Function (PDF) [43].

The Partially Premixed Combustion model is based on non-premixed and premixed combustion models. Therefore, in this model, thermochemistry is reduced to a single parameter, which is the mixture fraction

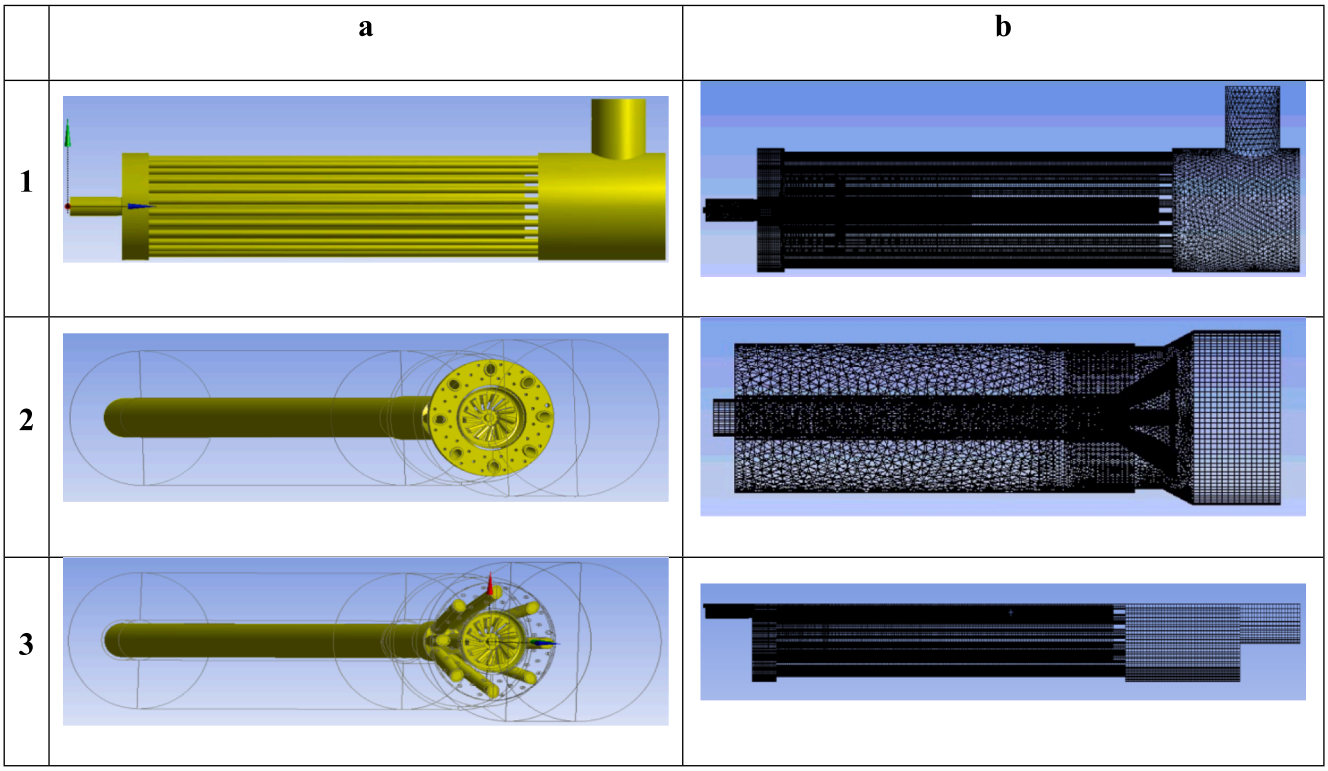


Fig. 2. 3D model of the boiler (a1), burner and swirl generator (a2, a3). The mesh structure of the complete volume with boiler (b1), the burner (b2) and the 1/4 (periodic) of the complete geometry (b3).

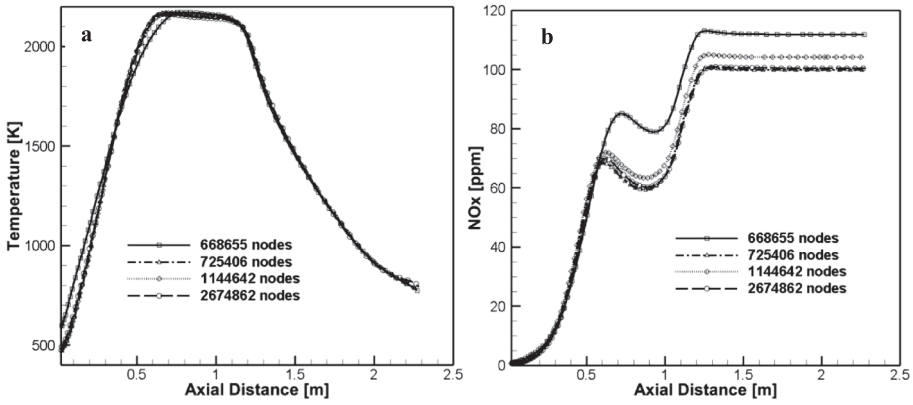


Fig. 3. NOx emission and temperature values on the boiler axis plane for different mesh numbers.

expression. In the case of a secondary fuel entering the reaction zone or a different component that may undergo a chemical reaction, the sum of the mixture fractions of the reactants must be equal to one [43].

3.3. 3D model and mesh structure

3D model of the boiler, burner and swirl generator are given in the Fig. 2a. Since the boiler and burner geometries are not suitable for 2D simulations, 3D simulations were carried out. In order to solve turbulent and complex flows, 3D simulations are more suitable. However, long simulation times and difficulties in convergence are some of the handicaps that need to be overcome. The mesh structure of the boiler and burner are given in Fig. 2b. The periodic model (1/4 model) was used to reduce the total number of meshes (Fig. 2b3).

Five models with different mesh structures (668655, 695374, 725406, 114642, and 2674862) were simulated for solution's independence of mesh size. From the simulation done with different mesh numbers, the results of NOx emission obtained from the boiler outlet are compared on the boiler axis line in Fig. 3.

It is seen that NOx emissions over the axial distance given in Fig. 3(a) vary significantly with the mesh number. It is thought that the reason for this difference is that NOx emissions are very sensitive to the temperature level and a small difference between temperatures causes significant differences in NOx. Despite this sensitivity, NOx levels are close to each other in the node numbers of 725406, 114,642 and 2674862. According to the results of the variation of the temperature given in Fig. 4 (b) with the axial distance, it is understood that the flame temperature tends to increase up to approximately 0.7 m from the exit of the burner. The temperature remained constant between 0.7 and 1.1 m and continued to decrease until the opposite wall of the hearth. The effect of the number of nodes on the boiler axis temperature is partially evident in the first section of the boiler. However, it is seen that it is not effective in

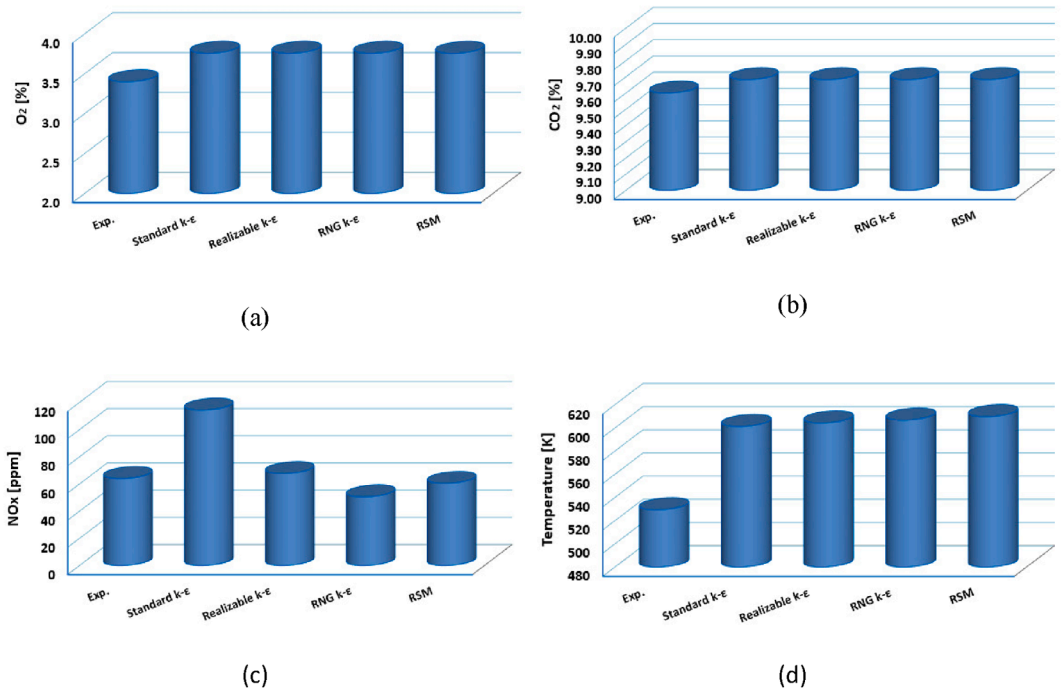


Fig. 4. Comparison of emissions (O_2, CO_2, NO_x) and temperature of CFD simulations using different turbulence models and experimental data.

the part where the axis temperature begin to decrease. Especially in the mesh numbers of 725406, 114,642 and 2674862, the temperature difference is almost negligible. Since the low mesh number significantly reduces the simulation time 725,406 number of mesh was preferred for all simulations.

3.4. Pysical properties, boundary conditions and solution method

ANSYS Fluent [43] commercial software was used for CFD simulations in this study. Since the fuel and air velocities at the burner inlet are less than Mach 0.2, the incompressible ideal gas was assumed for the CFD simulations [46]. For natural gas, the absorption and scattering coefficients was used as 0.5 [47] and 1e-09 [48] respectively. Mass flow was used as the burner inlet boundary conditions, while pressure output boundary conditions were defined for the boiler outlet. The realizable k-ε turbulence model was used to compare the combustion models due to the low eddy number that appeared ($S < 0.5$) in the burner. Optical thickness aL is a good tip for defining to use the appropriate radiation model between P1, Rosseland, Discrete Ordinates (DO) and Discrete Transfer (DTRM). Here a is the absorption coefficient and L is the length scale. In burner-boiler applications, L is equal to the combustion chamber's diameter. While it is recommended to use the Rosseland model for $aL \gg 1$ condition, P1 model for $aL > 1$ condition and DTRM and DO models for the $aL < 1$ condition [49]. Although the use of the DO model requires high computational cost, it can be preferred because of the many advantages, such as accounting for scattering, particulate effect, semi-transparent walls, specular walls, non-gray radiation, and localized heat sources [40]. In addition to all these advantages, the DO model was used for radiation calculations because $aL < 1$ condition at the current model.

The high degree of rotational flow resulting from swirl or rotation in the flow field causes large radial pressure gradients in the axial and radial directions. Such flows can cause instability in the solution process and cause the flow not to be fully modeled or the solution not to converge. PRESTO! scheme which is well-suited for detecting pressure gradients involved in swirling flows, may offer a solution strategy for swirling and swirling flows [40]. In this study, to discretize the three-dimensional flow field, PRESTO! is preferred, while COUPLED is used as pressure–velocity coupling. To describe the physics of the flow field, the Reynolds Avarage Navier-Stokes (RANS) equations for mass, momentum, energy and scalar transport are used under steady-state conditions.

4. Results and discussion

CFD simulation results from four different turbulence models were compared with the experimental results given in the first part of each section. The convergence of these models to experimental results for temperature and emissions has been investigated. Afterward, the results of simulations related to different combustion models are given together with the experimental results. According to all results, the most suitable turbulence and combustion models were suggested for natural gas fuel combustion CFD simulation in industrial low-swirl burners.

4.1. Investigation of the turbulence models

One of the critical factors for simulation combustion in CFD is defining the correct turbulence model. This choice is essential for the accuracy and reliability of the results. The effects of different turbulence models on temperature, NO_x, CO_2 and O_2 emissions at the boiler exhaust outlet are given in Fig. 4 by comparing with the experimental results. Here, $\%CO_2$ and $\%O_2$ levels from the experimental study obtained lower values than the CFD simulations. This difference is approximately 8% for CO_2 and 10.5% for O_2. (Fig. 4(a) ve (b)). In addition, it is seen that the turbulence models used do not make a significant difference in CO_2 and O_2 emission levels. The NO_x level measured in the experimental study and the NO_x levels calculated using different turbulence models are shown in Fig. 4(c). According to the CFD results, the Standard k-ε model predicts the NO_x level higher than the experimental and all other models. The error rate of the calculated value was 78.6% with experimental data. The realizable k-ε model result agrees well with the experimental data, while the error rate is 5.2%. The RSM model result is the second best result after the Realizable k-ε model, and the error rate is 5.6%. On the other hand, the RNG k-ε model results in NO_x emission lower than Realizable and RSM models, and the error rate of this model is calculated as 21%. As can be seen from these results, the Realizable k-ε

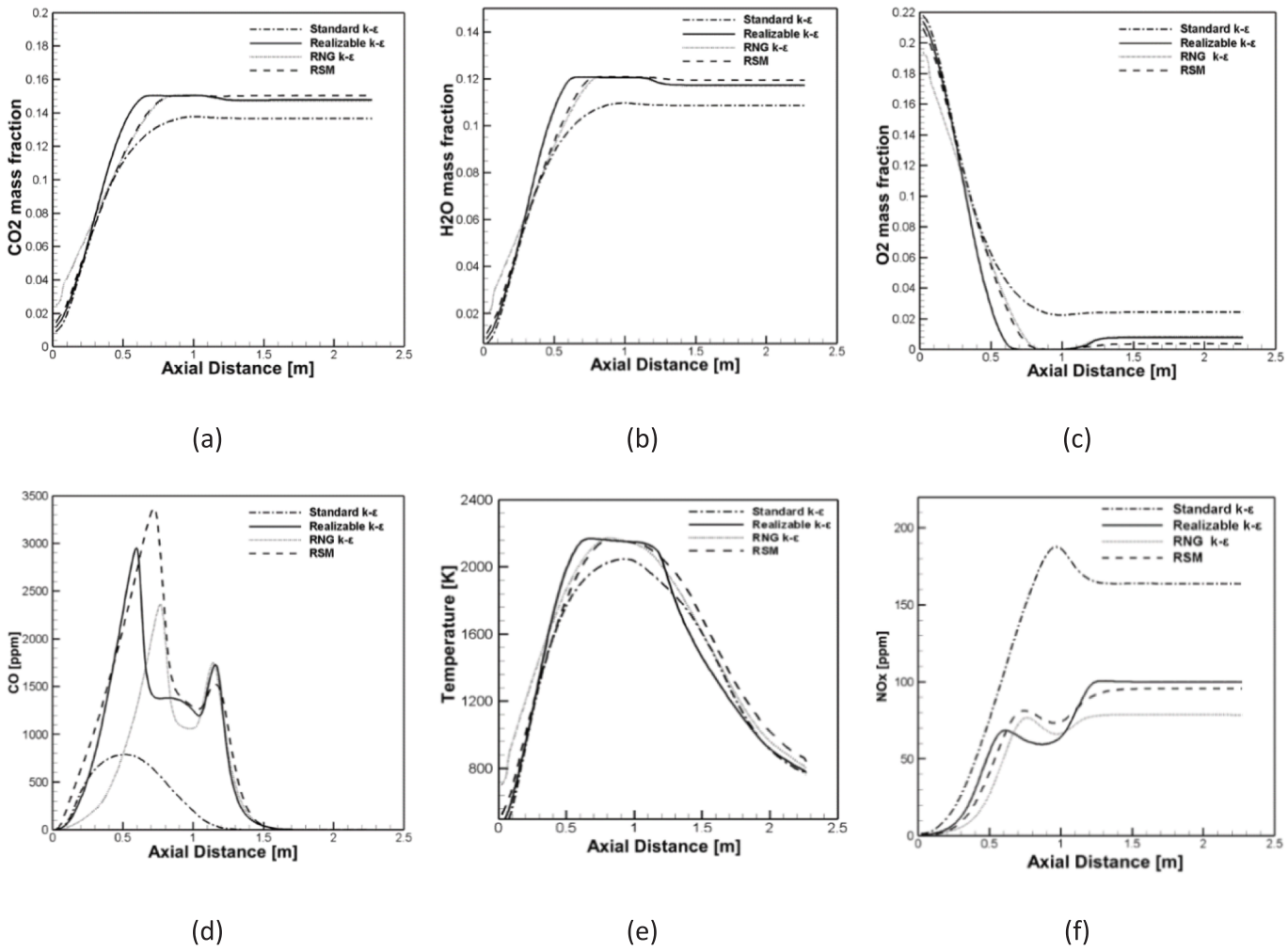


Fig. 5. Effect of turbulence models on emissions (CO_2, H_2O, O_2, CO, NO_x) and temperature along the boiler axis.

model gives better emission results than RNG k-ε and Standard k-ε models at low swirl number S < 0.5. Although the RSM model is recommended to be used at high swirl numbers (S > 0.5), it is seen to give good results at low swirl numbers. Therefore Realizable k-ε model is a good option for all simulations due to the better convergence with the experimental results. It is understood from the results that the experimental temperature results are lower than the CFD results. Temperature differences were calculated at approximately 13.5–15% between different turbulence models. In the experimental study, there are 26 curved turbulator and flue gas temperature-reducing sheet metal profiles in the chimney pipes. These structures couldn't include to CFD simulations due to the high mesh element requirement; therefore, there was a difference between the experimental and simulation temperature values.

The turbulent flow conditions in which each model is used are described in detail in the turbulence methods section. These methods are Standard k-ε, Realizable k-ε, RNG k-ε, and RSM models. Effect of different turbulence models in the solution of CO_2, H_2O, O_2, CO, temperature (T), and NO_x along the boiler axis distance are given in Fig. 5.

The CO_2 and H_2O results in the direction of the boiler axis are shown in Fig. 5 (a) and (b). Results shows that the increase of CO_2 and H_2O begins at the beginning of the burner, where the combustion reactions begin.

CO_2 and H_2O have constant trends between 0.8 m and 2.3 m and increasing trends between 0 m – 0.8 m. According to these results, the combustion process started with natural gas injection, and the amount of fuel reacted increased between 0 m – 0.8 m. After 0.8 m, the hydrocarbon value remained approximately constant throughout the axial distance. When the figures are examined, the turbulence models show the same trends for CO_2 and H_2O. The reason is the simultaneous formation of CO_2 and H_2O due to the combustion of hydrocarbons in a particular region.

CO_2 and H_2O emissions show a different trend for the RNG k-ε turbulence model in the burner inlet region (0–0.3 m) than other models. Besides the standard k-ε turbulence model in the 0.5–2.3 m range and the Realizable k-ε model has a different trend in the 0.3–0.7 m range. In addition, RNG k-ε and RSM models show the same trend between 0.3 m – 2.3 m, and RNG k-ε, Realizable k-ε and RSM models have very close values between 0.75 m and 2.3 m and maintain the same trend.

When the turbulence model trends for the O_2 mass fraction along the boiler axis distance in Fig. 5(c) are examined, a continuous decrease in the amount of O_2 entering the boiler is observed due to the reaction occurring from the boiler inlet. At the end of the flame around 0.8 m axis distance the amount of O_2 is almost exhausted for all turbulence models except Standard k-ε. Afterward, a slight increase is observed in the amount of O_2. This situation occurred similarly in the three turbulence models except Standard k-ε. In addition, the behavior of the turbulence models examined is just like the mass fractions of CO_2 and H_2O, and the same trends are exhibited at the same distances.

Fig. 5(d) shows the changes in the CO emissions along the axis distance of the boiler. From the figure, CO emissions increases with the initiation of combustion from the boiler entrance. Later CO emissions begins to decrease at 0.5 m distance for Standard k-ε after, 0.6 m distance for Realizable k-ε after, 0.7 m distance for RSM after, and 0.75 m

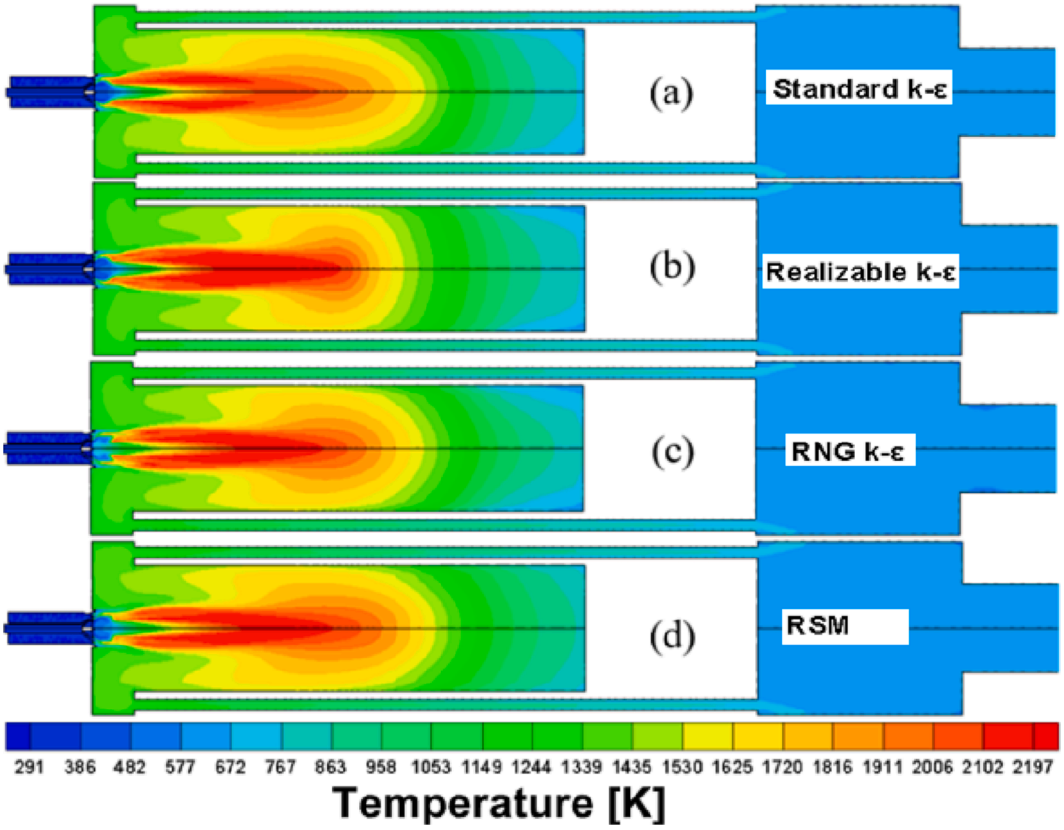


Fig. 6. Temperatures in the boiler axis plane using (a) Standard k − ε, (b) Realizable k − ε, (c) RNG k − ε and (d) RSM turbulence models.

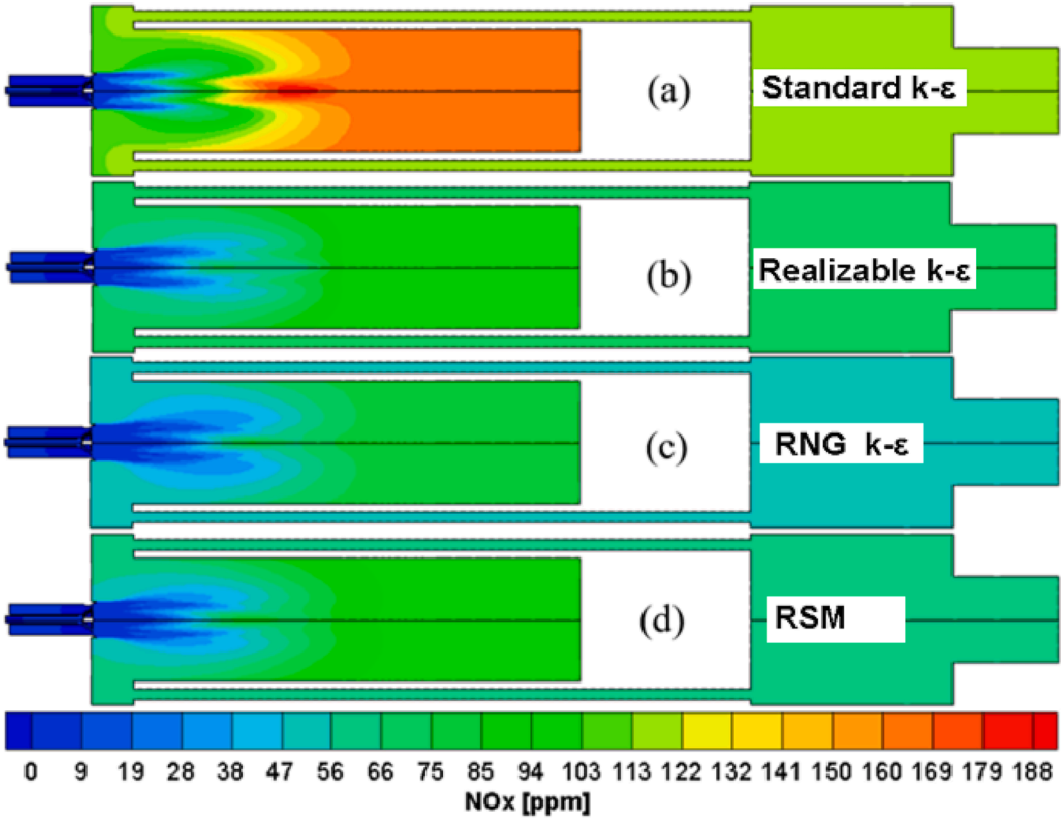


Fig. 7. NO_x emissions in the boiler axis plane using (a) Standard k − ε, (b) Realizable k − ε, (c) RNG k − ε and (d) RSM turbulence models.

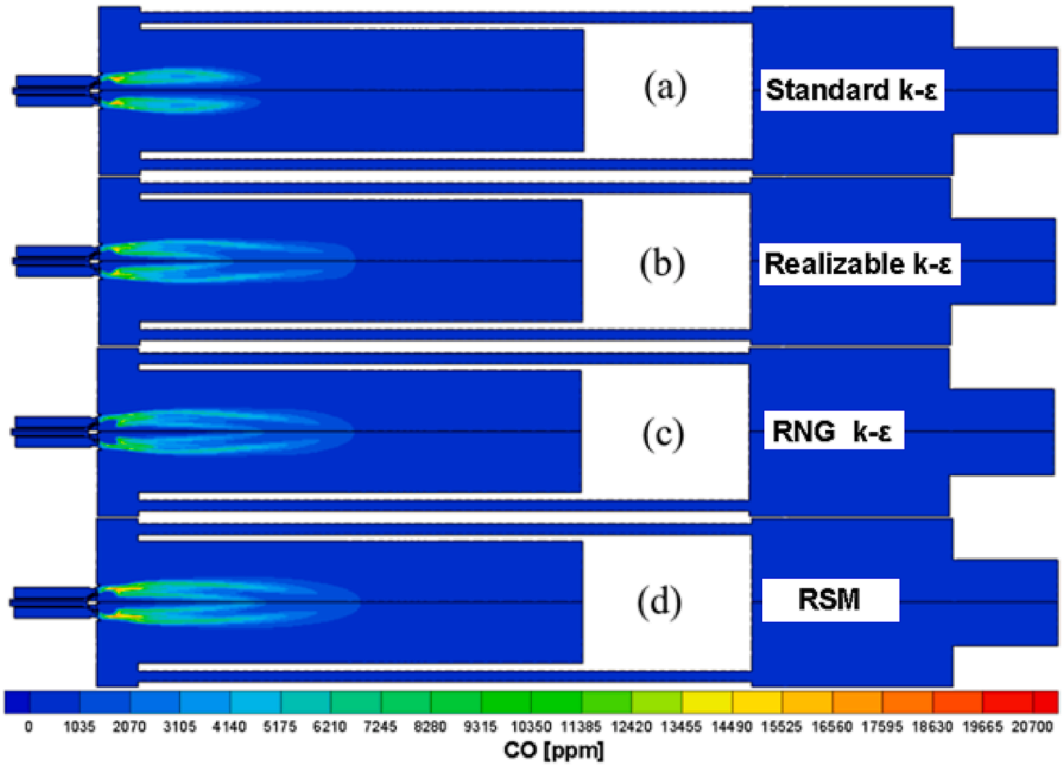


Fig. 8. CO emissions in the boiler axis plane using (a) Standard k − ε, (b) Realizable k − ε, (c) RNG k − ε and (d) RSM turbulence models.

distance for RNG k-ε model. There was a small increase in the CO emissions around the 1.2 m axial distance (except for the standard k-ε) and then decreased again.

Fig. 5(e) shows the temperature results along the axis distance from different turbulence models. According to the results obtained, it is seen that there is an increase in the boiler axis temperatures with the initiation of combustion from the inlet and the RNG k-ε model shows a different trend in this section (0–0.3 m). After z = 0.4 m, Realizable k-ε shows a different temperature profile. In the other three turbulence models, the temperature (standard k-ε, RNG k-ε and RSM) increases to an axial distance of approximately 0–0.8 m. After this interval, the temperature obtained from the turbulence models decreases parabolically and decreases to a certain temperature value (800–850 K) throughout the boiler. However, in the Realizable k-ε model, while the temperature increased between 0.4 m and 0.65 m, the temperature reached the highest (peak) value at 0.65 m, and immediately after that, the temperature slightly decreased linearly between 0.65 m-1.15 m. After a distance of 1.15 m, it decreases non-linearly to 800 K. In addition, the Realizable k-ε model calculated the axis temperature of the boiler after the flame at lower values than the other models. The maximum temperature values of the boiler axis were calculated closer each other and higher about 120 K than Standard k-ε model.

In Fig. 5(f), NO_x emission values are given for different turbulence models along the axis distance. NOx levels, which are sensitive to high-temperature values, can be significantly affected by small temperature changes. Therefore, in Fig. 5(e), besides the temperature changes along the distance of the axis, the local temperature values in the boiler affect NO_x emissions. In the standard k-ε turbulence model results, the NO_x emission was higher than the other models despite the low boiler temperature. The reason for this situation is that the maximum temperature in the boiler reached the highest value (2196.28 K) in the Standard k-ε model. In addition, NO_x emissions along the axis distance of the boiler with Standard k-ε show a different trend than other models and begin to increase from the boiler inlet. NO_x emission has the highest value (≈190 ppm) at z = 1 m, decreases slightly after this distance, and continues at a constant value (≈165 ppm) after z = 1.2 m distance. The other three models show similar trends but have different emission values. In all three models, the NO_x emissions increases from entry. In the realizable k-ε model, it is between 0.6 < z < 0.9 m. In RNG k-ε and RSM models, it decreases slightly in the range of 0.75 < z < 1 m and then increases again. After a distance of 1.2 m, NOx emissions continue at a constant value. Realizable k-ε (100 ppm) and RSM turbulence models (95 ppm) are close to each other for NOx emission along the boiler axial distance from the end of the flame zone. The results obtained from these models differ from the RNG k-ε turbulence model (80 ppm).

Fig. 6 shows the temperature distributions in the boiler by using four different turbulence models. As seen in the figure, flame forms are very similar in turbulence models other than the Realizable k − ε model, and the flames spread inside the boiler. The flame takes a more circular shape at the end of the flame in the realizable k − ε model. During combustion, the highest temperature value occurs in the Standard k − ε model (2196.28 K), while the lowest maximum temperature value occurs in the RSM model (2163.77 K). Approximately the same maximum temperature values (2173 K) were obtained in the Realizable and RNG k − ε models. While the longest flame form is created with the RSM model, the shortest form is formed by using the Realizable k − ε model. Flame diameters are close to each other. It is seen that the temperatures decrease towards the boiler outlet in each model.

NO_x emission formations were compared on the same scale using four different turbulence models in Fig. 7. When the figures are examined, it is seen that the highest NO_x level is obtained by using the Standard k − ε model, and the lowest value is formed by the RNG k − ε model. According to these data, it can be said that the turbulence models used and the maximum flame temperatures formed in the boiler are effective on NO_x but are not the only factors. Because while the maximum flame temperatures are the same in Realizable and RNG k − ε models, there is a 17 ppm difference between the NO_x values of these models.

Fig. 8 shows the changes in the CO emissions in the boiler from the inlet to the outlet. According to obtained data, it is seen that CO

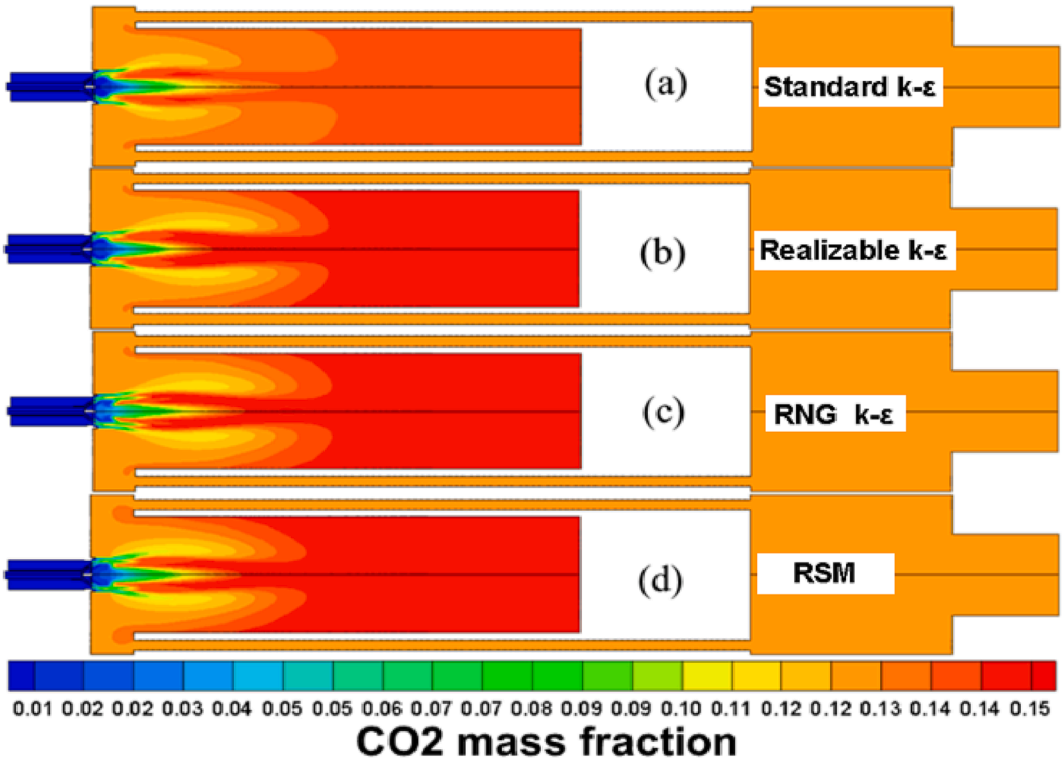


Fig. 9. CO_2 emissions in the boiler axis plane using (a) Standard k − ε, (b) Realizable k − ε, (c) RNG k − ε and (d) RSM turbulence models.

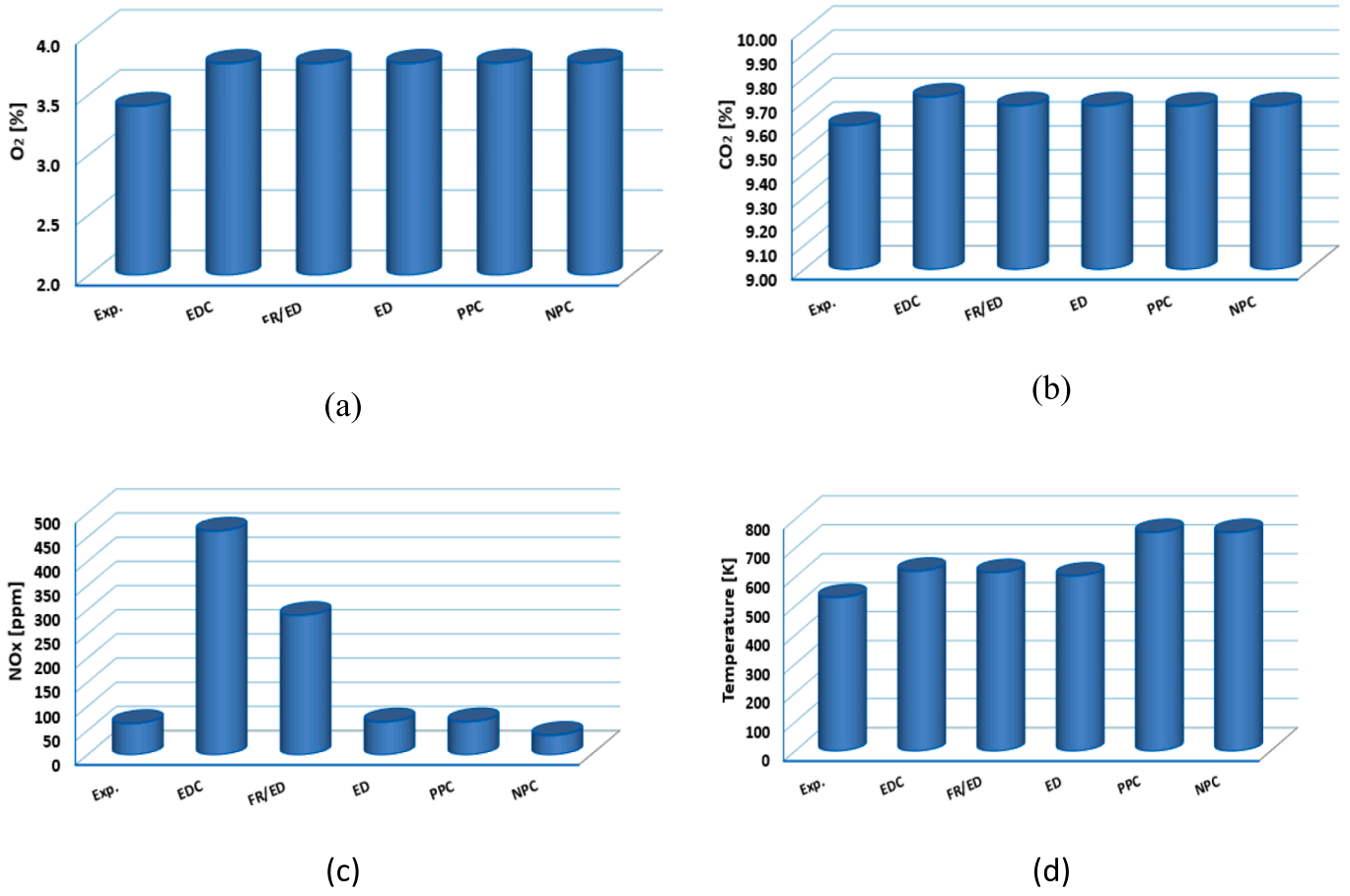


Fig. 10. Comparison of (a) temperature and combustion emissions (b) NOx, (c) CO_2 and (d) O_2 for CFD simulations using different combustion models and experimental study.

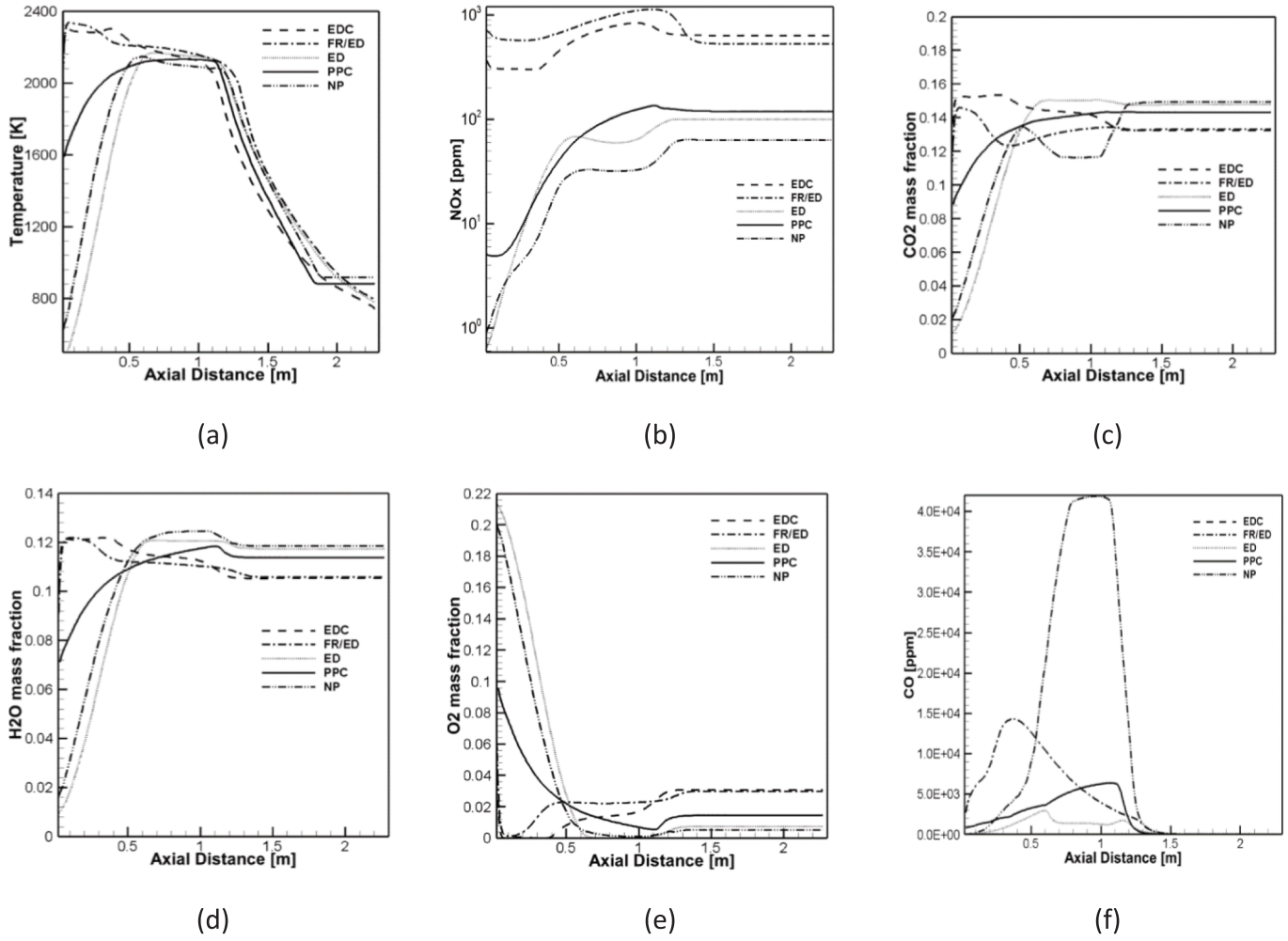


Fig. 11. Effect of combustion models on (a) temperature, (b)NO_x, (c) CO_2, (d) H_2O, (e)O_2 and (f) CO along the boiler axis.

emissions occur in the flame regions when there is oxygen deficiency, and these emissions are consumed outside the flame region by reacting to form CO_2 in the presence of oxygen atoms. In the case of using the standard k-ε model, it is seen that the amount of CO produced transforms in a shorter distance than the other models.

Fig. 9 shows the distribution of CO_2 emissions in the boiler when natural gas is modeled with four different turbulence models. According to the data obtained, while the CO_2 levels are similar to each other in models other than the Standard k-ε model, the CO_2 level formed in the flame region is lower in this model.

4.2. Investigation of combustion models

There are multiple combustion models available in the software and their selection depends on the fuel-oxidizer mixture type, laminar and turbulent flames, fast burning tendency of the fuel, whether the reaction can develop rapidly and the chemical kinetic mechanism used. For natural gas combustion EDC, FR/ED, ED, PPC and NPC combustion models were used with Realizable $k-\varepsilon$ turbulence model.

Fig. 10(a) shows the % O_2 amount, and Fig. 10(b) shows the % CO_2 amount in the combustion end gases. CFD showed that all emission results were higher than the experimental results. Error rates are up to 1.76% for CO_2 emissions with the EDC model and for O_2 emissions up to 7.44% with the NPC model. The emission levels of NOx, one of the most important combustion emissions, are shown in Fig. 10(c). As can be seen from the figure, the EDC and FR/ED models estimated the NOx level much higher than the experimental data. The error rates of these two models are 611% and 342.73%, respectively. On the other hand, the NPC combustion model provided the lowest NOx estimation, including the experimental result. According to the experimental result, the error rate of this model is 39%. The ED and PPC models are the most compatible with the experimental results regarding NOx emission in the analyses made with different combustion models according to the experimental operating conditions. The error rates in these two models are 3.66% and 4%, respectively. Fig. 10(d) gives the boiler gas outlet temperatures that ED model is closest to the experimental study. In the EDC and FR/ED models, on the other hand, despite the very high flame temperatures, the gas outlet temperatures are close to the gas outlet temperature calculated in the ED model. On the other hand, gas outlet temperature values in PPC and NPC models were close. According to these results, all models predict high gas outlet temperatures. One reason is that turbulence-increasing plates in the curved structure of smoke pipes required high mesh elements and weren't included in the simulation.

The temperature distributions along the axis of the boiler for five different combustion model results are shown in Fig. 11(a). ED and NPC combustion models exhibit similar temperature curves from the boiler inlet. It is seen that the temperatures gradually increase in the range of $0 < z < 0.6$ m and follow a curve close to linear. In addition, the higher temperature was obtained for the ED model in this region of the NPC combustion model. EDC and FR/ED combustion models other than these two models show similar temperature changes along the axis distance of the boiler. For these two models, it is seen that the combustion begins at the boiler inlet (at the burner end) and reaches high-temperature values.

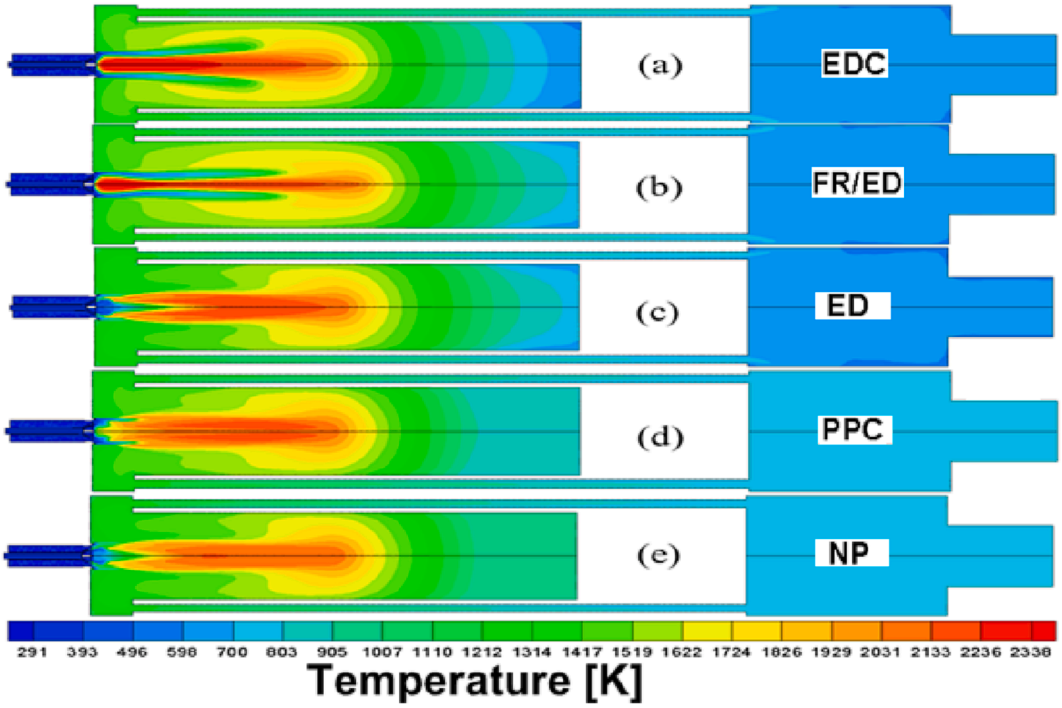


Fig. 12. Temperature distributions in the boiler axial plane by using different combustion models ((a) EDC, (b) FR/ED, (c) ED, (d) PPC and (e) NP).

After the flame temperatures reach their peak values in a very short distance, there is a gradual decrease towards the end of the flame (z = 1.2 m). It is observed that the axis temperatures decrease sharply, especially after z > 1.2 m distance. In the PPC model, like the EDC and FR/ED models, the combustion starts at the boiler inlet (at the burner end), but in the PPC model, the boiler axis temperature is lower than these two models. In addition, the temperature increase in this model showed a slower and decreasing increase compared to the ED and NPC models from the boiler inlet. In all models, temperatures drop sharply to approximately 1.1 m < z < 1.2 m. This is because this range is where the flames formed end. It can be explained by the gradual decrease in temperature in the axis of the boiler due to the end of the combustion in this region. Especially after a distance of z = 1.18 m, the temperature remains constant in the PPC and NPC models, while the temperatures continue to decrease until the opposite wall of the boiler in the other three models. After the gap where the flame form ends, ED and FR/ED showed the same trend in the region up to the opposite wall of the boiler. PPC and NPC show a similar trend. Although the EDC model is similar to the ED and FR/ED models, it is quite different in terms of the values it receives.

NO_x emission on the boiler axis of different combustion models is directly proportional to the boiler axis temperature levels. The reason for this is, as mentioned before, high-temperature regions and the residence time in these regions have an increasing effect on NO_x formation. Fig. 11(b) shows the NO_x variation along the boiler axis distance for each combustion model. In the examination, ED and NPC combustion models show similar tendencies with other combustion models. From the boiler inlet, NO_x levels increase gradually with the development of combustion for both models. It continues at a constant value of 0.5 < z < 1.2 m. NO_x levels continue at a constant value for z > 1.2 m. However, using the ED combustion model, the NO_x emission is estimated to be higher than in the NPC combustion model. The difference between the PPC combustion model from these two models is that since the combustion process is more advanced from the burner end, higher NO_x emission occurs from these two models from the inlet. By quarry axis distance, it usually makes higher estimates than either model. Although the PPC combustion model shows a similar trend along the boiler axis to the two models, it offers a different behavior from both models in the 0.5 < z < 1.2 m. On the other hand, when using EDC and FR/ED models, NO_x values are higher than all other combustion models due to high flame temperatures. Although the tendencies of these two combustion models are similar, NO_x values remain lower in the flame region with the EDC model but remain at higher levels after the flame than in the FR/ED model.

The analysis results of the CO_2 and H_2O emissions resulting from the combustion of natural gas on the boiler axis line are given in Fig. 11(c) and (d) for different combustion models. The tendencies of the CO_2 and H_2O products formed during the combustion of natural gas are very similar along the boiler axis line. The most obvious difference is the mass fraction values. CO_2 emission decreases between 0.5 < z < 1 m, while H_2O emission increases in this range in the NPC combustion model. The effects of different combustion models on the CO_2 and H_2O formation processes are very similar to temperature changes in the 0 < z < 0.5 m. While the temperatures drop sharply after the endpoint of the flame in the axial temperature change (Fig. 11 (a)), the CO_2 and H_20 formation curves continue at a constant value after this point. On the other hand, CO_2 and H_2O emissions of the quarry in the range of 1.2 m < z < 2.3 m are highest in NPC and ED models and lowest in EDC and FR/ED models. On the other hand, CO_2 and H_2O emissions of the quarry in the range of 1.2 m < z < 2.3 m are highest in NPC and ED models and lowest in EDC and FR/ED models.

Fig. 11(e) and (f) show the mass fraction of O_2 and CO emissions results. O_2 was consumed at a shorter distance in EDC and FR/ED combustion models with the development of combustion at the inlet of the burner. And then it started to rise again suddenly afterward. The O_2 emission gradually decreases with the gradual development of combustion along the boiler axis from the boiler inlet in OED and NPC combustion models. The PPC model of the combustion process shows behavior between these four models. O_2 emissions have a similar trend among these models and are average. EDC combustion model exhibits a different situation from other combustion models in terms of CO emission. There wasn't any CO formation on the boiler axis line in the EDC combustion model. This model performs natural gas combustion as a complete combustion process. CO emission on the boiler axis line is very

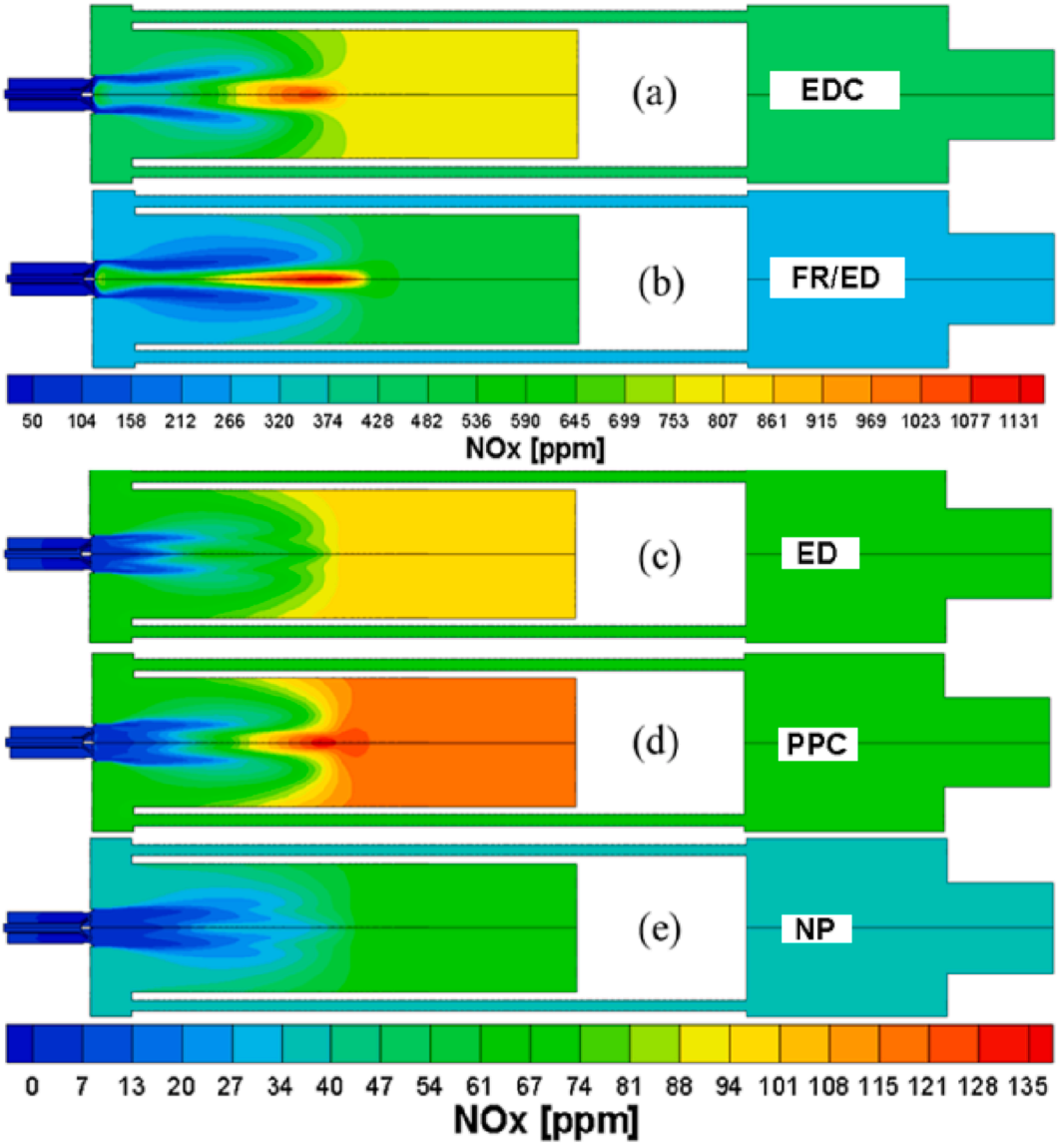


Fig. 13. NO_x distributions in the boiler axial plane by using different combustion models ((a) EDC, (b) FR/ED, (c) ED, (d) PPC and (e) NP).

low in the ED combustion model. The CO emission in the PPC combustion model is approximately two times higher than in the ED combustion model. Similarly, it disappears after the flame. On the other hand, according to the FR/ED model, in the region close to the boiler entrance, the CO level reaches its maximum value in the $0 < z < 0.37$ m. Subsequently, it gradually decreases towards the end of the flame and is consumed. Finally, in the NPC combustion model, the CO level increases logarithmically from the boiler inlet. At a distance of $z = 1$ m, the CO value takes its maximum value and then decreases sharply, and the flame is finally exhausted.

The 2D visual temperature distributions obtained in the boiler are shown in Fig. 12. It is seen that the temperatures formed in the flame zone by using the EDC and FR/ED models are higher than the ED, PPC, and NPC models. This is because the natural gas mechanism has two-step reaction in EDC and FR/ED models. Since the formation of many intermediates expected to occur under normal conditions was neglected, the specific heats are higher than the actual heat. However, the temperatures formed by using PPC and NP models at the end of the boiler outlet area are higher than EDC, FR/ED, and ED models.

Fig. 13 shows the variation of NO_x emissions. Since the NO_x level formed by using the EDC and FR/ED combustion models is much higher than the other models, two different colour scales were used. NO_x emissions obtained by using the EDC (a) and FR/ED (b) models were compared with first scale. NO_x emissions obtained in the ED, PPC and NPC models were compared with the second scale. When the figures are examined, NO_x formations can be seen in the flame core region in EDC, FR/ED and partially PPC models. This is not seen in ED and NPC models. It is observed that NO_x levels outside the core region remain at constant values due to the lower temperatures in these regions and the completion of NO_x formation mechanisms. In the examination, it is seen that while the highest NO_x emission is obtained with the EDC model, the lowest NO_x emission is obtained by using the NPC model.

Another reason for obtaining the highest temperature and NO_x levels in the EDC model can be seen as the presence of sufficient oxygen in the flame zone due to excess air. This situation is also evident from the low CO level in the EDC model in Fig. 14. When the figure is examined, it is seen that EDC Model CO emission remains at very low levels compared to other models due to the excess amount of oxygen. CO levels vary with the use of other models, and the highest CO level is obtained with the NP model. The least formation NOx is seen in the NP model, and it cannot predict the combustion better than other combustion models. For this reason, it has been the model with the highest CO emission. Almost 4000 ppm of CO emissions are seen in the flame region.

Fig. 15 shows the CO_2 emissions from natural gas combustion for

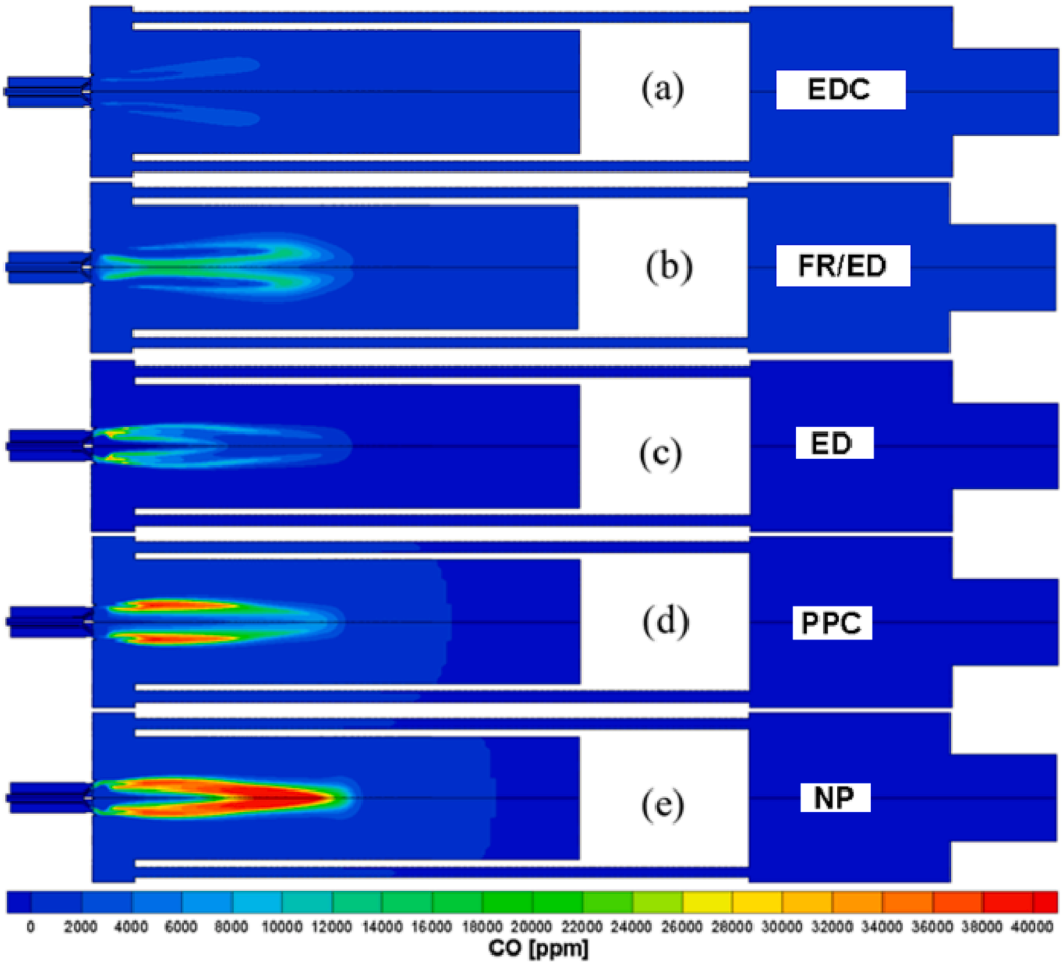


Fig. 14. CO distributions in the boiler axial plane by using different combustion models ((a) EDC, (b) FR/ED, (c) ED, (d) PPC and (e) NP).

different models. In EDC and FR/ED models, intense CO_2 formation is observed from the burner inlet, while CO_2 formation is observed in the further distances of the boiler in the other three models. It is also seen that the output CO_2 levels are close to each other.

5. Conclusion

In this study, emissions and temperature values were obtained from a low swirl natural gas burner for $\lambda = 1.2$ at a 1085 kW thermal load using experimental and CFD simulation methods. It was aimed to determine the most suitable turbulence and combustion model between Standard k $-$ ε, Realizable k $-$ ε, RNG k $-$ ε, RSM turbulence models and Eddy Dissipation Model (ED), Finite Rate/Eddy Dissipation (FR/ED), Eddy Dissipation Concept (EDC), Partial-Premix Combustion (PPC), Non-Premix Combustion (NPC) combustion models.

The results obtained from simulations can be listed as follows:

- As a result of simulations using different turbulence models, the Realizable k $-$ ε was the most suitable for NO_x estimation in modeling the low swirl natural gas burner. The realizable k $-$ ε model was developed for rotation, recirculation, and swirl flow modeling. And it is an enhanced version of the Standard k $-$ ε model. Therefore, the Realizable k $-$ ε model can predict the eddy flow in the burner relatively better than others. For this reason, it can calculate the temperature distribution along with the flow more accurately; therefore, the thermal NO_x mechanism can also make a more accurate NO_x solution. Since other models cannot model these backflows, they can predict higher temperature values in these regions and, therefore, high NO_x values.
- As a result of CFD analyses using different combustion models, it was understood that Partial-Premix Combustion (PPC) model best fits the NO_x experimental data.
- Since the two-step chemical mechanism for natural gas used in EDC and FR/ED models neglects the formation of many intermediate products that are expected to occur under normal conditions. Since the specific heats are higher than the standard value, the simulations made with these models have reached a higher combustion temperature in the core region of the flame. For this reason, CFD results of NO_x values are much higher than the experimental results for EDC and FR/ED combustion models.
- At the temperature distributions results in the boiler axial plane, the highest temperature was obtained from the Standard k $-$ ε model (2196.28 K), at the same time, the lowest (120 K lower than the other turbulence models) temperature value obtained along the boiler axis from Standard k $-$ ε model. Therefore, the Standard k $-$ ε model shows differences for CO_2, H_2O, O_2, CO, and NO_x results than other turbulence models.

Declaration of Competing Interest

The authors declare that they have no known competing financial interests or personal relationships that could have appeared to influence the work reported in this paper.

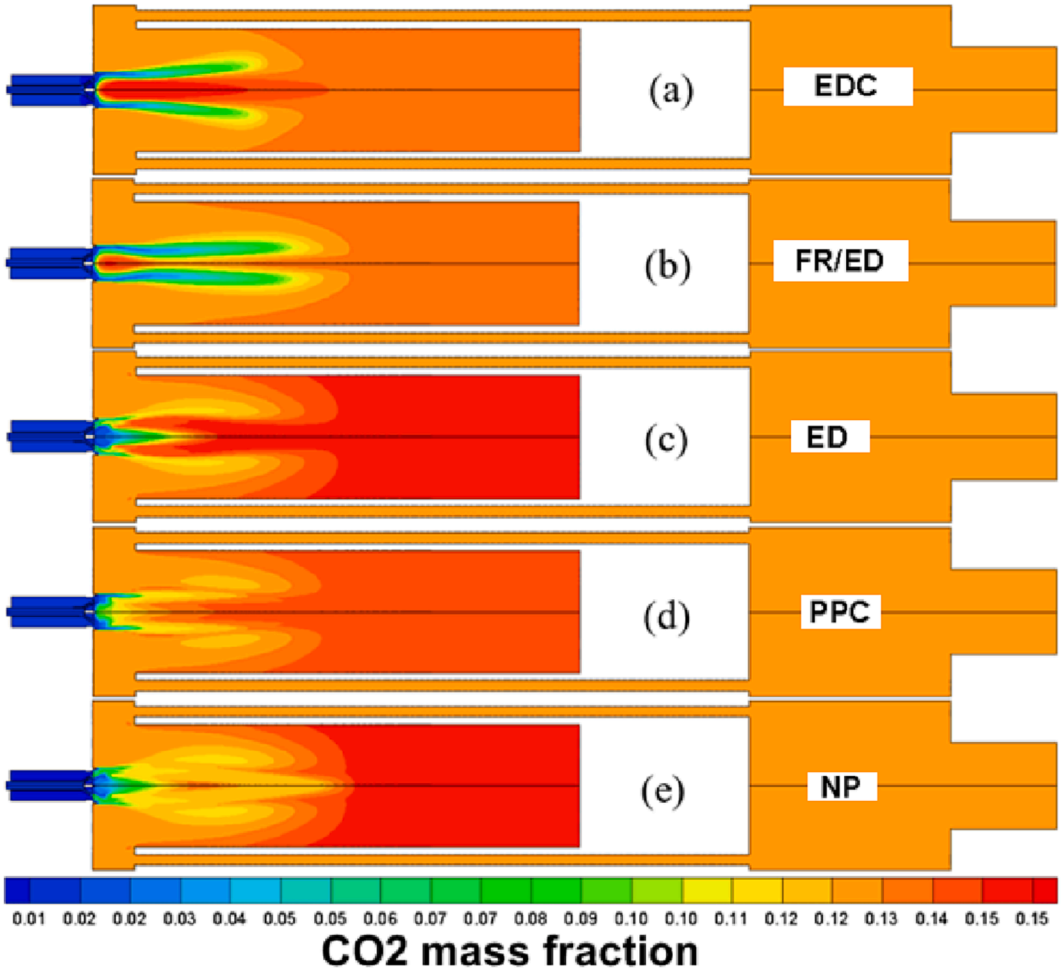


Fig. 15. CO_2 distributions in the boiler axial plane by using different combustion models ((a) EDC, (b) FR/ED, (c) ED, (d) PPC and (e) NP).

Data availability

The authors do not have permission to share data.

Acknowledgment

This study is derived from the Ph.D. Thesis titled "Investigation of combustion emissions in an industrial type burner-boiler system" supported by Yıldız Technical University Teknopark and Termo-Heat Isı San.A.Ş. We would like to thank both institutions and their employees.

References

[1] Energy Information Administration U. International Energy Outlook 2016 2040.
[2] Chanphavong L, Zainal ZA. Characterization and challenge of development of producer gas fuel combustor: a review. J Energy Inst 2019;92:1577–90. https://doi.org/10.1016/J.JOEI.2018.07.016.
[3] Connolly BM, Madden DG, Wheatley AEH, Fairen-Jimenez D. Shaping the future of fuel: monolithic metal-organic frameworks for high-density gas storage. J Am Chem Soc 2020;142:8541–9. https://doi.org/10.1021/JACS.0C00270/ASSET/IMAGES/MEDIUM/JA0C00270_0006.GIF.
[4] Safari A, Das N, Langhelle O, Roy J, Assadi M. Natural gas: a transition fuel for sustainable energy system transformation? Energy Sci Eng 2019;7:1075–94. https://doi.org/10.1002/ESE3.380.
[5] Sahu C, Kumar R, Sangwai JS. Comprehensive review on exploration and drilling techniques for natural gas hydrate reservoirs. Energy Fuel 2020;34:11813–39. https://doi.org/10.1021/ACS.ENERGYFUELS.0C02202/SUPPL_FILE/EF0C02202_SI_001.PDF.
[6] Bertelsen N, Mathiesen BV. EU-28 Residential Heat Supply and Consumption: Historical Development and Status. Energies 2020, Vol 13, Page 1894 2020;13:1894. https://doi.org/10.3390/EN13081894.
[7] Ziemele J, Talcis N, Osis U, Dace E. A methodology for selecting a sustainable development strategy for connecting low heat density consumers to a district heating system by cascading of heat carriers. Energy 2021;230:120776. https://doi.org/10.1016/J.ENERGY.2021.120776.
[8] Chen W, Shang S, Wang B, Li X, Cao Y, Shi W. Experimental study on effects of supply-air humidification on energy and emission performance of domestic gas boilers. Energy Build 2020;209:109726. https://doi.org/10.1016/J.ENBUILD.2019.109726.
[9] Gómez MA, Martín R, Chapela S, Porteiro J. Steady CFD combustion modeling for biomass boilers: an application to the study of the exhaust gas recirculation performance. Energy Convers Manag 2019;179:91–103. https://doi.org/10.1016/J.ENCONMAN.2018.10.052.
[10] Bohlooli Arkhazloo N, Bouissa Y, Bazdidi-Tehrani F, Jadidi M, Morin JB, Jahazi M. Experimental and unsteady CFD analyses of the heating process of large size forgings in a gas-fired furnace. Case Stud Therm Eng 2019;14:100428. https://doi.org/10.1016/J.CSITE.2019.100428.
[11] Brundage AL, Burl Donaldson A, Gill W, Kearney SP, Nicolette VF, Yilmaz N. Thermocouple Response in Fires, Part 1: Considerations in Flame Temperature Measurements by a Thermocouple. Http://DxDoiOrg/101177/0734904110386187 2010;29:195–211. https://doi.org/10.1177/0734904110386187.
[12] Yilmaz N, Gill W, Donaldson AB, Lucero RE. Problems encountered in fluctuating flame temperature measurements by thermocouple. Sensors (Basel) 2008;8:7882. https://doi.org/10.3390/S8127882.
[13] Yilmaz N, Burl Donaldson A, Edward Lucero R. Experimental study of diffusion flame oscillations and empirical correlations. Energy Convers Manage 2008;49:3287–91. https://doi.org/10.1016/J.ENCONMAN.2007.10.035.
[14] Brundage AL, Burl Donaldson A, Gill W, Kearney SP, Nicolette VF, Yilmaz N. Thermocouple Response in Fires, Part 2: Validation of Virtual Thermocouple Model for Fire Codes. Http://DxDoiOrg/101177/0734904110386188 2010;29:213–26. https://doi.org/10.1177/0734904110386188.
[15] Yilmaz N. Detailed multiphysics modeling and validation of thermocouple readings in fires. Http://DxDoiOrg/101177/0734904111405303 2011;29:443–64. https://doi.org/10.1177/0734904111405303.
[16] Rossiello G, Uzair MA, Ahmadpanah SB, Rogora M, Saponaro A, Torresi M. Integrated use of CFD and field data for accurate thermal analyses of oil/gas boilers. Fuel 2023;335:126931. https://doi.org/10.1016/J.FUEL.2022.126931.
[17] Littlejohn D, Cheng RK. Fuel effects on a low-swirl injector for lean premixed gas turbines. Proc Combust Inst 2007;31(2):3155–62.

[18] El-Sherif AS. Effects of natural gas composition on the nitrogen oxide, flame structure and burning velocity under laminar premixed flame conditions. Fuel 1998;77:1539–47. https://doi.org/10.1016/S0016-2361(98)00083-0.
[19] Ren Z, Goldin GM, Hiremath V, Pope SB. Simulations of a turbulent non-premixed flame using combined dimension reduction and tabulation for combustion chemistry. Fuel 2013;105:636–44. https://doi.org/10.1016/J.FUEL.2012.08.018.
[20] Belcadi A, Assou M, Affad EH, Chatri EH, Belcadi A, Assou M, et al. CH4/NOx reduced mechanisms used for modeling premixed combustion. Energy Power Eng 2012;4:264–73. https://doi.org/10.4236/EPE.2012.44036.
[21] Kang Yinhu, Lu Xiaofeng, Wang Quanhai, Ji Xuanyu, Miao Shanshan, Xu Jie, et al. Experimental and modeling study on the flame structure and reaction zone size of dimethyl ether/air premixed flame in an industrial boiler furnace. Energy Fuel 2013;27(11):7054–66.
[22] Cuoci A, Frassoldati A, Faravelli T, Ranzi E, Candusso C, Tolazzi D. CFD simulation of a turbulent oxy-fuel flame 2010. https://doi.org/10.4405/PTSE2010.VII4.
[23] Ilbas M, Yilmaz I, Veziroglu TN, Kaplan Y. Hydrogen as burner fuel: modelling of hydrogen–hydrocarbon composite fuel combustion and NOx formation in a small burner. Int J Energy Res 2005;29:973–90. https://doi.org/10.1002/ER.1104.
[24] Yilmaz I, Taştan M, Ilbaş M, Tarhan C. Effect of turbulence and radiation models on combustion characteristics in propane–hydrogen diffusion flames. Energy Convers Manag 2013;72:179–86. https://doi.org/10.1016/J.ENCONMAN.2012.07.031.
[25] Ilbaş M, Karyeyen S, Yilmaz I. Effect of swirl number on combustion characteristics of hydrogen-containing fuels in a combustor. Int J Hydrogen Energy 2016;41:7185–91. https://doi.org/10.1016/J.IJHYDENE.2015.12.107.
[26] Johnson MR, Littlejohn D, Nazeer WA, Smith KO, Cheng RK. A comparison of the flowfields and emissions of high-swirl injectors and low-swirl injectors for lean premixed gas turbines. Proc Combust Inst 2005;30(2):2867–74.
[27] Strakey P, Sidwell T, Ontko J. Investigation of the effects of hydrogen addition on lean extinction in a swirl stabilized combustor. Proc Combust Inst 2007;31(2):3173–80.
[28] Borsuk A, Williams J, Meadows J, Agrawal AK. Swirler effects on passive control of combustion noise and instability in a swirl-stabilized combustor. J Eng Gas Turbine Power 2015:137. https://doi.org/10.1115/1.4028613/373170.
[29] Bebar L, Kermes V, Stehlik P, Canek J, Oral J. Low NOx burners—prediction of emissions concentration based on design, measurements and modelling. Waste Manage 2002;22:443–51. https://doi.org/10.1016/S0956-053X(02)00028-4.
[30] Schmittel P, Günther B, Lenze B, Leuckel W, Bockhorn H. Turbulent swirling flames: experimental investigation of the flow field and formation of nitrogen oxide. Proc Combust Inst 2000;28:303–9. https://doi.org/10.1016/S0082-0784(00)80224-6.
[31] Silva C v., Vielmo HA, França F. NUMERICAL SIMULATION OF THE COMBUSTION OF METHANE AND AIR IN A CYLINDRICAL CHAMBER. Thermal Engineering 2006;5:13–21.
[32] Ren Z, Goldin GM, Hiremath V, Pope SB. Simulations of a turbulent non-premixed flame using combined dimension reduction and tabulation for combustion chemistry. Fuel 2013;105:636–44. https://doi.org/10.1016/J.FUEL.2012.08.018.
[33] Frassoldati A, Sharma P, Cuoci A, Faravelli T, Ranzi E. Kinetic and fluid dynamics modeling of methane/hydrogen jet flames in diluted coflow. Appl Therm Eng 2010;30:376–83. https://doi.org/10.1016/J.APPLTHERMALENG.2009.10.001.
[34] Ziani L, Chaker A, Chetehouna K, Malek A, Mahmah B. Numerical simulations of non-premixed turbulent combustion of CH4–H2 mixtures using the PDF approach. Int J Hydrogen Energy 2013;38:8597–603. https://doi.org/10.1016/J.IJHYDENE.2012.11.104.
[35] Pfeiler C, Raupenstrauch H. Application of different turbulence models to study the effect of local anisotropy for a non-premixed piloted methane flame. Comput Aided Chem Eng 2010;28:49–54. https://doi.org/10.1016/S1570-7946(10)28009-4.
[36] Khaldi N, Mhiri H, Bournot P. A comparative study of turbulence models performance for a 300 MWe tangentially fired pulverized-coal furnace. IREC 2014 - 5th International Renewable Energy Congress 2014. https://doi.org/10.1109/IREC.2014.6826960.
[37] Cellek MS, Pınarbaşı A. Investigations on performance and emission characteristics of an industrial low swirl burner while burning natural gas, methane, hydrogen-enriched natural gas and hydrogen as fuels. Int J Hydrogen Energy 2018;43:1194–207. https://doi.org/10.1016/J.IJHYDENE.2017.05.107.
[38] ANSYS Inc. (2015). ANSYS Fluent Theory Guide-Release 16.0, Canonsburg, USA. n. d.
[39] Launder BE, Spalding DB. The numerical computation of turbulent flows. Comput Methods Appl Mech Eng 1974;3:269–89. https://doi.org/10.1016/0045-7825(74)90029-2.
[40] Fluent Inc., (2005). Fluent 6.2 User Guide, 2A. n.d.
[41] Inc. F. Fluent 6.2 User Guide, 2A. Fluent Inc.; 2005.
[42] Yılmaz İ. Model Bir Yakıcıda Hidrojen-Metan Karışımının Yanmasının Sayısal Ve Deneysel İncelenmesi. Erciyes Üniversitesi Fen Bilimleri Enstitüsü, Kayseri: Doktora Tezi; 2006.
[43] ANSYS Fluent Theory Guide-Release 16.0. n.d.
[44] Spalding DB. Mixing and chemical reaction in steady confined turbulent flames. Symp (Int) Combust 1971;13:649–57. https://doi.org/10.1016/S0082-0784(71)80067-X.
[45] Bakker A. Modeling Chemical Reactions with CFD, Reacting Flows - Lecture 10 2006. http://www.bakker.org/dartmouth06/engs199/10-react.pdf (accessed September 27, 2017).
[46] Colorado A, McDonell V. Prediction of NOx emissions from premixed natural gas and hydrogen enriched flames stabilized with a low-swirl burner. Fall Technical Meeting of the Western States Section of the Combustion Institute, WSS/CI 2013 Fall Meeting 2013.
[47] Ilbas M. The effect of thermal radiation and radiation models on hydrogen-hydrocarbon combustion modelling. Int J Hydrogen Energy 2005;30:1113–26. https://doi.org/10.1016/j.ijhydene.2004.10.009.
[48] FLUENT13.0 A. Tutorial: 2D Simulation of a 300 KW BERL Combustor Using the Magnussen Model. 2010.
[49] Fluent Inc. Choosing a Radiation Model 2006. https://www.sharcnet.ca/Software/Fluent6/html/ug/node583.htm (accessed September 28, 2017).